Received May 21, 2021, accepted June 6, 2021, date of publication June 14, 2021, date of current version June 23, 2021.

Digital Object Identifier 10.1109/ACCESS.2021.3089358

Severity Assessment of Social Anxiety Disorder Using Deep Learning Models on Brain Effective Connectivity

ABDULHAKIM AL-EZZI[1], NORASHIKIN YAHYA[1], (Member, IEEE), NIDAL KAMEL[1], (Senior Member, IEEE), IBRAHIMA FAYE[1], (Senior Member, IEEE), KHALED ALSAIH[2], (Member, IEEE), AND ESTHER GUNASELI[3]

[1]Centre for Intelligent Signal and Imaging Research (CISIR), Electrical and Electronic Engineering Department, Universiti Teknologi PETRONAS, Seri Iskandar 32610, Malaysia
[2]Université de Lyon, UJM-Saint-Etienne, CNRS, IOGS, Laboratoire Hubert Curien UMR5516, F-42023 Saint-Etienne, France
[3]Psychiatry Discipline Sub Unit, Universiti Kuala Lumpur Royal College of Medicine Perak, Ipoh 30450, Malaysia

Corresponding author: Norashikin Yahya (norashikin_yahya@utp.edu.my)

This work was supported in part by the Ministry of Higher Education Malaysia under Higher Institutional Centre of Excellence (HICoE) Scheme awarded to Centre for Intelligent Signal and Imaging Research (CISIR), and in part by the Yayasan Universiti Teknologi PETRONAS under Grant YUTP-FRG 015LC0-292.

This work involved human subjects or animals in its research. Approval of all ethical and experimental procedures and protocols was granted by the Medical Research Ethics Committee of the Royal College of Medicine Perak, Kuala Lumpur University, under Approval No. UniKLRCMP/MREC/2019/065, and performed in line with the Helsinki Declaration.

ABSTRACT Neuroimaging investigations have proven that social anxiety disorder (SAD) is associated with aberrations in the connectivity of human brain functions. The assessment of the effective connectivity (EC) of the brain and its impact on the detection and medication of neurodegenerative pathophysiology is hence a crucial concern that needs to be addressed. Nevertheless, there are no clinically certain diagnostic biomarkers that can be linked to SAD. Therefore, investigating neural connectivity biomarkers of SAD based on deep learning models (DL) has a promising approach with its recent underlined potential results. In this study, an electroencephalography (EEG)-based detection model for SAD is constructed through directed causal influences combined with a deep convolutional neural network (CNN) and the long short-term memory (LSTM). The EEG data were classified by applying three different DL models, namely, CNN, LSTM, and CNN + LSTM to discriminate the severity of SAD (severe, moderate, mild) and healthy controls (HC) at different frequency bands (delta, theta, alpha, low beta, and high beta) in the default mode network (DMN) under resting-state condition. The DL model uses the EC features as input, which are derived from the cortical correlation within different EEG rhythms for certain cortical areas that are more susceptible to SAD. Experimental results revealed that the proposed model (CNN + LSTM) outperforms the other models in SAD recognition. For our dataset, the highest recognition accuracies of 92.86%, 92.86%, 96.43%, and 89.29%, specificities of 95.24%, 95.24%, 100%, and 90.91%, and sensitivities of 85.71%, 85.71%, 87.50%, and 83.33% were achieved by using CNN + LSTM model for severe, moderate, mild, and HC, respectively. The fundamental contribution of this analysis is the characterization of neural brain features using different DL models to categorize the severity of SAD, which can represent a potential biomarker for SAD.

INDEX TERMS Effective connectivity network, convolutional neural networks (CNNs), social anxiety disorder (SAD), default mode network (DMN), deep learning models, partial directed coherence (PDC), electroencephalogram (EEG), human brain mapping.

I. INTRODUCTION

Social anxiety disorder (SAD) is a widespread and debilitating syndrome marked by anxious emotions of negative appraisal or criticism in social events [1]. SAD is primarily diagnosed based on clinical indications and medical biomarkers, but its pathophysiology is mostly uncharted. Therefore, it is necessary to recognize efficient and thematic biomarkers to differentiate individuals with SAD from healthy controls (HCs) and other anxiety disorders [2].

The associate editor coordinating the review of this manuscript and approving it for publication was Vishal Srivastava.

Human psychological SAD can be quantified using subjective and quantitative assessments. Subjectively, the severity of SAD is evaluated using surveys (created by the specialists) or interviews performed by an experienced psychologist [3]. Quantitatively, SAD is perceived using somatic, clinical, and biological techniques. Symptoms can be evident in the form of facial indications, eye blinking rates, and dilated pupils in the physical measurements of SAD [4]. Currently, SAD is commonly identified on the basis of clinical symptoms, self-assessment reports, and pathophysiology, which may either be inaccurate or falsely reported. Therefore, it is important to utilize effective and appropriate measures to characterize the severity of SAD. Different biomarkers including heart rate (HR) and electrocardiogram (ECG), electrodermal response, and EEG were used to assess the severity of SAD [5].

Recently, resting-state functional magnetic resonance imaging (MRI) has gained significant popularity in investigating mental illness states. The fMRI mechanism not only managed to overcome possible drawbacks correlated with task frameworks in other modalities but also it is likewise fairly straightforward. However, fMRI is relatively costly and has a poor temporal resolution compared to other modalities, and its data are highly sensitive to head movements. Alternatively, the data provided by EEG presents an instantaneous measure of the underlying neural activities with a high temporal resolution of few milliseconds. These unique characteristics, in addition to being non-invasive and cost-effective, makes EEG a preferable module for studying the electrophysiological and cognitive states of the human brain [6], [7].

Traditionally, neuroscientists have often used superficial models, for example, support vector machine (SVM), as classifiers for the identification of emotional states (e.g., SAD) and for performing certain analyses [8]. However, when confronted with challenging classification tasks, these superficial models have some restrictions on understanding the intrinsic features of training data [9]. Recently, in many fields, the DL approach has been used widely to recognize features and effectively identify different types of data. Convolutional neural networks (CNNs) are responsive to spatially dispersed influences and can be applied to estimate the categorical data, segregating patients with SAD from HCs, and prognosticating the severity of SAD bio-indexes at individual levels [10]. There are various DL architectures, such as deep belief networks, recurrent neural networks (RNN), CNN, and LSTM. Primarily, a DL model is used to reduce the size of the EEG data and then convert them into new descriptions without any noticeable loss of intrinsic information. Several studies have used CNN models in various types of EEG classification tasks, such as emotional discrimination [11], time-frequency analysis [12], epileptic seizure classification [13], and Parkinson's disease [14]. Another study has briefly clarified that a CNN with its deep feed-forward design exhibits a superior capability to generalize as compared to a CNN with fully connected layer networks [15]. Owing to the high performance in image classification, identification of objects, brain seizure detection, speech identification, diabetic retinopathy, and other applications, CNNs are being increasingly used in numerous fields [15]. Consequently, the integration of emotional identification and deep models is believed to be a promising research subject for the improvement of emotional recognition accuracy and practicability [16]. In addition to CNN, Long short-term memory (LSTM) is an artificial RNN model applied in the domain of DL models. In contrast to the other DL models, LSTM processes the entire series of data (such as continuous EEG) [17]. The only reported analysis on LSTM is that of [18], which is restricted to only two data classifications (SAD and depression data); moreover, it was applied to speech audio data and not to EEG data. Thus far, to the best of our knowledge, no EC studies have been reported on the implementation of DL models to determine the severity of patients with SAD from HCs. Such research is essential to examine whether data for EC obtained using PDC could serve as a therapeutic diagnostic technique of SAD, with assertiveness on early medication. Features derived from the PDC, a linear measurement of EC is used in the automatized prediction of three classes of SAD versus HC using the CNN + LSTM deep model, thus resulting in high classification accuracy [19]. We applied a deep CNN model to classify the three classes of SAD (severe, moderate, and mild), and HC, in which convolution and atrous convolution operations were performed considering one LSTM layer utilized. The presentation of the proposed deep model is explained in sectionIV. It should be noted that as compared to the ML models, DL has considerably enhanced the performance of many classification models. Previous studies have reported different FC of SAD patients as compared to HCs [20]. Therefore, we hypothesized that EC data and deep models could also be used as a possible index to differentiate between the classes of SAD and HC. In addition, we also hypothesized that abnormal resting-state EC may be implicated in the social cognition process and emotional regulation. We expected that by investigating the DMN brain in particular, we might be able to gain sufficient knowledge to advance our understanding of the pathophysiology of SAD.

The primary aim of this study is to extend the previous literature by utilizing the CNN + LSTM classification model with effective neural brain information in the DMN. Further, we examined the possibility of a correlation between DMN brain regions that largely assisted in high accuracy classification and symptom severity in the SAD groups. The chosen features were utilized to identify the perceived SAD into three different classes and compare them with HCs. The central contributions of this research are as follows:

1) A new collection of EEG dataset comprises 22 HC subjects, 22 mild, 22 moderate, and 22 severe SAD subjects, respectively, which will be made publicly available for further studies on SAD and mental health-related conditions.
2) Development and evaluation DL models for 3-class classification of SAD severity level based on effective

connectivity of cortical regions in DMN extracted from EEG signals.

The remainder of this paper is structured as follows. Section II describes the resting-state and DMN, presenting the cortical regions involving in. Section III is discussing the concept of effective connectivity in neuroscience. Section IV describing the data preprocessing procedure that is applied to raw EEG data, along with an explanation of the mechanism for computation of the EC matrices. Moreover, the methodology for the features extraction is also presented in addition to an explanation of the raw EEG data utilized in this research and of how these attributes were converted into multidimensional images as CNN input using the proposed CNN + LSTM architectures. Section V presents the statistical analysis and experimental results. The discussion along with study limitations also were discussed in the same section V. Finally, the paper conclusion is presented in Section VI.

II. DEFAULT MODE NETWORK

Neuroscience suggests that the DMN is able to contribute to the neuropsychological investigation of cognitive and social functionality, which can assist in delineating the neural biomarkers of SAD. The DMN is evidenced to play a major role in coordinating cognitive processing, such as self-reflection, retrieval of memories, and many functions that are known intuitionally as mind-wandering [21], [22]. DMN impairment is found to be involved in some mental pathology conditions, including autism [23], Alzheimer's disease [24], and depression [25]. Moreover, this dysfunction can serve as the foundation of self-information regulation and emotional process bias in the SAD [26]. The resting-state functional connectivity (FC) features in the DMN of SAD patients and HCs were compared and the findings revealed that the FC between different cortical regions in the aged people was greater than in the youths [19]. Furthermore, the influence of SAD on the prefrontal brain was estimated using structural and functional MRI studies [27]. Specifically, in HCs and SAD individuals, a variance was observed in the resting-state FC between the hippocampus and the limbic-prefrontal circuit in the DMN network [28]. The DMN has revealed greater connectome in the resting-state when an individual was more focused internally rather than externally or on attention-demanding tasks [29].

III. EFFECTIVE CONNECTIVITY

The effective connectivity in resting-state (absence of any external stimuli) is a robust and definitive analysis technique in which the concurrent activities of brain neurons can be investigated without any stimuli [30], [31]. The DMN is one of the optimum networks that are frequently recognized in resting-state EC studies. The dominant regions of the DMN imply the medial prefrontal cortex (mPFC), posterior cingulate cortex (PCC)/precuneus, and lateral parietal cortex (LPC) [22], [32]. Originally, essential regions within the DMN, i.e., mPFC, Anterior cingulate cortex (ACC), PCC, and insular [33] are prime for emotional regulation processing, because they represent these neural circuits as putative candidates for the investigation of emotion regulation aberration in SAD. Several SAD analyses have revealed resting-state connectivity aberration in the brain regions within the DMN [34], [35] and the amygdala connectivity in patients with SAD [36], [37]. A review on resting-state neuroimaging in SAD [38] exhibited wide connectome variations between limbic areas and DMN regions correlated with SAD. They concluded that future analyses are recommended for studying the connectivity alterations within the DMN in subjects with SAD. Contemporary studies showed decreased functional fMRI connectivity in the right mPFC, dorsolateral prefrontal cortex (DLPFC), precuneus, and the right inferior parietal gyrus compared with HCs (DMN regions), thus indicating that SAD is accompanied by dysfunction in cognitive processing [39]–[41]. FC examines the statistical dependencies between the estimated neurophysiological activities. Conversely, EC indicates the effect that a neuron exceeds another using the connection model of causal brain flow. Furthermore, EC is always directed and relies on an evident model of causal effects. Generally, EC is estimated using either variance (discrete-time) or differentiation (continuous-time) equations. The most common method of obtaining EC is the dynamic causal modeling (DCM) [42]–[44]. In this approach, causality is engrained in the model, wherein the oscillations in hidden neurons affect the alterations in other neurons. For instance, in certain regions, the oscillations in neurophysiological signals are influenced by information from other regions. Granger causality (GC), which identifies directed connections from time-series data, presents itself as an effective and widely used statistical method that locates natural implementation in neuroscience studies. EC is commonly estimated using different tools, including DCM, [45], phase slope index [46] partial directed coherence (PDC), and directed transfer function (DTF). PDC and DTF are frequency-domain methods based on the multivariate autoregressive model (MVAR) and the principle of GC [45], [47]–[49]. In this analysis, we have applied PDC to estimate the directed coherence between two signals while neglecting the volume conduction (insensitive to noise).

In this study, we used EEG signals to explore the severity of SAD through variations in the information flow between different regions of the brain in the DMN. These variations in the EC over the DMN regions were fed into a specially designed DL network for the assessment of SAD severity into four levels (HC, mild, moderate, and severe).

IV. MATERIALS AND METHODS

In this section, we explain the adopted methods during the preparation of the original EC matrices, the transformation of sensory information into cortical DMN activity, the source reconstruction, and the measures are taken to increase the number of appropriate social anxiety patterns to achieve improved classification accuracy. We also discussed the participants' information, the experimental paradigm, data acquisition, and data preprocessing, respectively.

A. PARTICIPANTS

We recruited 89 participants from 502 respondents who recorded their self-assessment reports of the SIAS. Both genders were included in the experiment to generalize the results of the research and to validate the data findings of our analysis. All subjects were assessed using the SIAS scale to determine the severity state of SAD. Accordingly, the participants were assigned to four different categories: HC (SAIS score < 20), mild (SIAS score < 40), moderate (SIAS score < 60), and severe (SIAS score 60). Later, one subject was excluded due to data acquisition problems. Age did not exhibit any significant differences between the groups, $F(1, 87) = 2{,}664$, $p = 054$, $\eta^2 = 0.093$. All participants were right-handed (to generalize hemisphere dominance), mentally and physically healthy, with no signs of brain damage. None of the respondents had any history of psychiatric, neurological, or surgical disabilities, which may impair brain function or metabolic functions. During the recruitment process at the time of the EEG session, no subjects were found to receive any pharmacological or psychotherapeutic medication. According to self-reports, all participants had a normal or corrected-to-normal vision. A single sheet including all study details and a waiver of written informed consent was provided to all selected participants with an honorarium to compensate them for their time and cooperation. Table 1 represents the demographic data and participants' characteristics.

B. EEG DATA ACQUISITION AND EXPERIMENTAL DESIGN

To examine whether the SAD states are being represented appropriately, we developed a social performance task for SAD assessment to acquire EEG data that could generate substantial and original datasets. The social performance task was reported in our previous studies [50], [51]. In our studies, we have ensured proper consideration of the time factor and cooperative behaviors of the participants. The resting-state recordings were conducted completely at the EEG laboratory. Participants were instructed to be seated comfortably, with their eyes closed, in a quiet, mid-dark room, and let their minds wander freely; EEG resting-state data were recorded for approximately 6 min. First, participants were required to refrain from drinking caffeine and alcohol at least 4 h prior to their EEG recording. After the electrodes were placed on the scalp, we followed the EEG protocol to record the resting state of the EEG for 6 min. Finally, they were asked to respond to the self-report questionnaires and were discharged. The protocol for this research has been carefully reviewed, accepted, endorsed, and approved by the Medical Research Ethics Committee of the Royal College of Medicine Perak, Kuala Lumpur University, and was performed in accordance with the Helsinki Declaration [52].

C. EEG PREPROCESSING

Real-time EEG data were consistently collected during a six-minute baseline term using a referential 32-channel shielded cap (ANT Neuro, Enschede, Netherlands). All 32

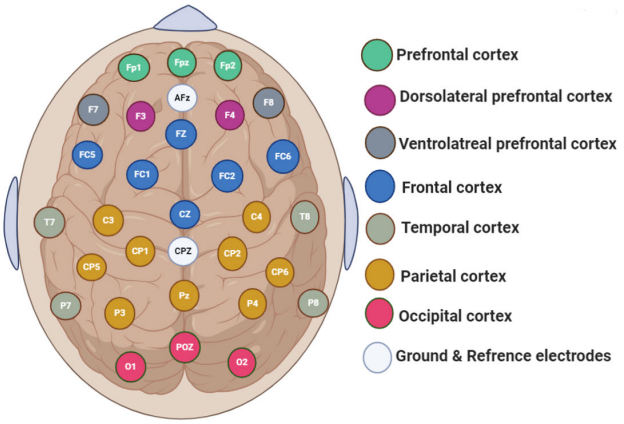

FIGURE 1. Topographical placement of 32 electrodes using the extended international system 10-20, indicating the distribution of the electrodes on the cortical scalp.

gel-based sensors were mounted on the EEG head cap and referenced to CPz and grounded at AFz. The recorded EEG signals were then re-referenced to a common average reference. The impedance was maintained below 10kΩ. The electrophysiological information was recorded at a sampling rate of 2048 Hz and was later downsampled to 256 Hz. Fig. 1 shows the topographic distribution of EEG electrodes in the cortex identified as prefrontal (Fp1, Fp2), medial prefrontal (mPFC: Fpz), ventro-lateral prefrontal (F7, F8), dorso-lateral prefrontal (F3, F4), frontal (FC5, FC1, FC2, FC6), mid-frontal (Fz, Cz), temporal (T7, T8, P7, P8), parietal (C3, C4, CP5, CP1, CP2, CP6, P3, P4), mid-parietal (Pz), occipital (O1, O2), and mid-occipital (POz). To eliminate the high-frequency electrocortical artifacts, signal noise, and low-frequency deflections, we applied an FIR band-pass filter to acquire the signal segment between the frequency range of 0.4 and 50 Hz. In accordance with the international standards, EEG signals were acquired from numerous active sensors (electrodes) attached to the cerebral cortex with a constant spatial arrangement. Artifacts such as eye blinks, horizontal (HEOG), and vertical (VEOG) eye motions, breathing, power interference, and cardiac movements were visually inspected and automatically discarded using spatial filters based on artifact detection and correction provided by BESA software.

D. SOURCE LOCALIZATION BASED ON EFFECTIVE CONNECTIVITY

Our datasets are forward models in which they can explain how the electrical potential sources determine the brain activity values on the EEG electrodes. This is a practically effective mechanism for simulations, but more importantly, is how to estimate the electrical potential generators of the EEG activities (inverse problem) from the EEG recordings. For that purpose, we have computed the source localization for the 32-electrode EEG to determine the current distribution of the predominant sources of the brain activity associated with SAD, in our study only at the cortical level. he source

TABLE 1. Demographic data and group characteristics.

Group	Number of participants		Total	Age		SIAS score	
	Female	Male		Female	Male	Female	Male
Severe	12	10	22	22.13 ± 2.78	23.11 ± 1.02	67.53 ± 6.21	66.81 ± 5.32
Moderate	7	15	22	21.98 ± 3.11	22.21 ± 1.25	55.7 3± 7.81	54.41 ± 6.61
Mild	12	10	22	22.61 ± 2.32	21.71 ±2 .31	38.32 ± 512	37.71 ± 5.81
Control	8	14	22	21.76 ± 1.73	23.62 ± 1.65	14.71 ± 6.74	16.61 ± 7.34

TABLE 2. EEG electrode (s) of default mode network regions with its corresponding MNI coordinates and Brodmann regions.

ROI	MNI coordinates			Anatomical regions	BA
	X	Y	Z		
FZ	0.6	40.9	53.9	Central mPFC	8-9-10
F3	-35.5	40.9	32.1	Left mPFC	8-9-10
F4	40.2	47.6	32.1	Right mPFC	8-9-10
PZ	0.2	62.1	64.5	PCC/ Precuneus	7
P3	39.5	76.3	47.4	Left LPC	39–40
P4	38.8	74.9	49.2	Right LPC	39–40
CP4	62	42	32	Left Parietal Lobe	40
CP6	66	34	40	Right Parietal Lobe	40

model of Minimum norm imaging (MNI) implemented in brainstorm toolbox [53], [54] was applied. The cerebral region coordinates are constructed based on the Montreal Neurological Institute average MRI brain map (MNI) with 15000 vertices of the cortex surface as reported in [55]. The method determines a cortical current dipole source density image that approximately fits the data when mapped through the forward model [56].

We have excluded the non-active cortical areas from further statistical EC analysis. Eight (8) ROIs were found to be active among all subjects (e.g., F3, F4, Fz, CP6, CP4, P3, P4, and Pz) which are located in the DMN regions. The time EEG sources computed from the localized EEG waveforms were then exported as mean activity in the effective connectivity analysis. Directed connectivity weights between these active regions were calculated for each artifact-free EEG segment in the following frequency bands: delta (1–3 Hz), theta (4–8 Hz), alpha (9–12 Hz), low beta (13-22) and high beta (23–30Hz). The same procedure was extended to the entire drive-data. Moreover, for each channel, the EC components and power spectral densities derived from the MVAR models were computed at the scalp current source density level for each participant. In order to facilitate the calculation of the average matrices, the measured power spectra were normalized before the data were averaged. For the DMN state, in particular, the measured power spectra for all participants are specified by averaging delta, theta, alpha, low beta, and high beta. Moreover, Analysis of variance (ANOVA) [57] was performed to check the statistical difference between the EC values in the emotional states of SAD in a given frequency band. Furthermore, the values of the main diagonal were excessive because they indicated that each region was concurrent to itself, and hence, they were ignored by the analysis. The entire process is illustrated in Fig. 2. Table 2 presents the most active DMN regions along with their Brodmann areas (BA).

E. EFFECTIVE CONNECTIVITY

To train a classification model, we applied effective connectivity features for precision-based SAD prediction based on PDC algorithm. PDC is a frequency domain technique based on the MVAR and the concept of partial coherence and GC. Neuroscientists have long used the GC approach for multichannel datasets, including EEG data [49]. The GC concept reveals that if a neural signal $Y(t)$ implies information in past values that assist in the prediction of neural signal $X(t)$, $Y(t)$ is believed to cause $X(t)$.

The PDC is applied to the DMN-related regions for the estimation of the effective connections between them, using MATLAB code generated by Baccala and Sameshima [58]. The PDC provides another estimation technique for the association between a pair of neuronal signals, which defines the correlation between regions i and j. The PDC from channel j to channel i indicates the directional flow of information from one activity site in the ROI to another. As mentioned earlier, these PDC values are in the range of [0, 1] [58]. Generally, an MVAR model with a number of cortical DMN regions (m ROIs) of EEG signals and order p is defined as follows:

$$Y(t) = [y_1(t), y_2(t), \ldots, y_n(t)]^T, \tag{1}$$

is represented by an autoregressive model of order p as given in Equation (2)

$$Y(t) = \sum_{l=1}^{p} \mathbf{A}_l \mathbf{Y}(t-l) + \boldsymbol{\varepsilon}(t), \tag{2}$$

where,

$$\mathbf{A}_l = \begin{bmatrix} a_{11}(l) & \cdots & a_{1n}(l) \\ \vdots & \ddots & \vdots \\ a_{n1}(l) & \cdots & a_{nn}(l) \end{bmatrix}, \tag{3}$$

is the coefficient matrix at the time lag l. $X(t)$ represents the weight vector of m ROIs of EEG signals at time t, matrix $A(r)$ indicates the r^{th} order AR parameters, and $E(t)$ represents the measured error that is believed to be an independent Gaussian process with zero mean. When the coefficients of the MVAR model are adequately calculated, $A(F)$ is determined as follows:

$$A(F) = \sum_{r=1}^{p} \mathbf{A}_r e^{-i2\pi fr}, \tag{4}$$

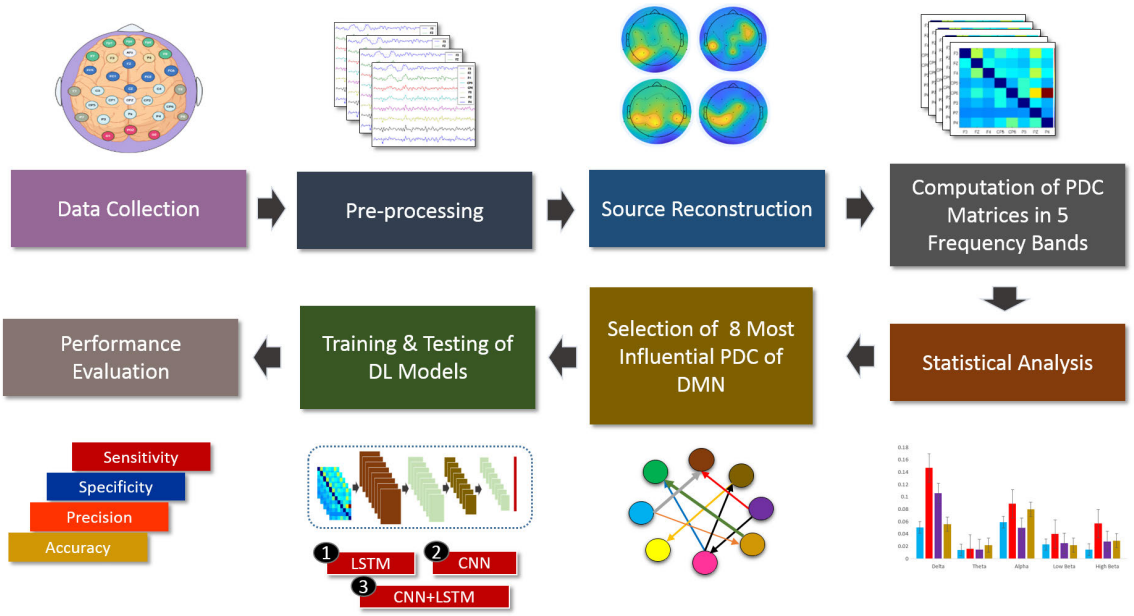

FIGURE 2. Block diagram for the EEG data analysis module to identify the parameters of the EC network and application of deep learning models.

Therefore, the PDC value from channel j to channel i can be expressed as follows:

$$PDC_{ij} = \frac{A_{ij}(\bar{f})}{\sqrt{a_j - \bar{H}(f)\bar{a}_j(f)}}, \tag{5}$$

where, $(\bar{a}_i)(f)$ $(i = 1, 2, \ldots M)$ represents the i^{th} column of the matrix $\bar{A}(f)$ and PDC_{ij} represents the directional influence and intensity of the information flow from channel j to channel i at a frequency of f. The PDC values were computed for each combination and used as an input feature for the classifiers. Features from these frequency bands were chosen to provide optimum accuracy with optimal order at $p =$ 5-7 [59], [60]. In our case, the optimum order is 5.

The calculation of the PDC matrix for each frequency band was obtained using continuous 3-second segments of EEG recording. Since the duration of the EEG signal for each subject is 180 seconds, a total of 60 (8×8)-PDC matrices are obtained for each frequency band. Therefore, the PDC matrices for each subject from 5 frequency bands are equal to 300.

F. DEEP NEURAL NETWORKS

In our analysis, three deep models, namely, LSTM, CNN, and a mix of CNN and LSTM were trained using EC that belongs to the DMN regions. The averaged spectral EC was extracted from five frequency bands, namely, delta, theta, alpha, low beta, and high beta. For each participant, the (8×8)-PDC matrices from 5 bands are combined to be the input to the CNN and CNN + LSTM models for ease of exposition and without loss of generality, as illustrated in Fig. 3. However, since LSTM takes in series input, the (8×8)-PDC matrix for each band is first converted to 1D vector and then combined to form a 320-length 1D vector. To ensure equal class balance, EEG recordings from 22 participants are used for each class giving a total of 88 participants for all 4 classes.

CNN is a class of DL models; specifically, it is a multilayer perceptron with several convolution-pooling layers and fully connected layers at the output. Input features are convolved with multiple-dimensional filters in the convolution layer and sub-sampled to produce a smaller scale in the pooling layer. Shared network weights and filters in the convolution layer are learnable through the backpropagation algorithm, which minimizes the classification errors. As shown in Fig. 3, the LSTM model has two LSTM layers, followed by a fully connected layer and a classification layer, namely softmax, to classify the 4-class outputs. Hidden units (HU) of 110 and 90 were utilized for the first and second hidden layers, respectively. Moreover, the model was regularized by applying dropout layers after each LSTM layer to avoid model overfitting with a ratio of 0.20.

The second proposed deep architecture is a CNN-based model, which consisted of a mix of vanilla and atrous convolution operations. The reason behind utilizing atrous convolution is the wider range covered by them in comparison to vanilla operations. For example, a 3×3 atrous convolution filter with a dilation rate of 2 is equal to a 5×5 filter in the vanilla operations. Hence, the spatial region grows wider while the parameter number remains constant. Therefore, more meaningful feature maps are expected to be generated for the benefit of enhancing SAD classifications. After each convolution of the atrous convolution layer, a batch normalization layer and ReLU layer are applied.

In the CNN and CNN + LSTM models, the difference occurs in the max-pooling and average-pooling layer stride

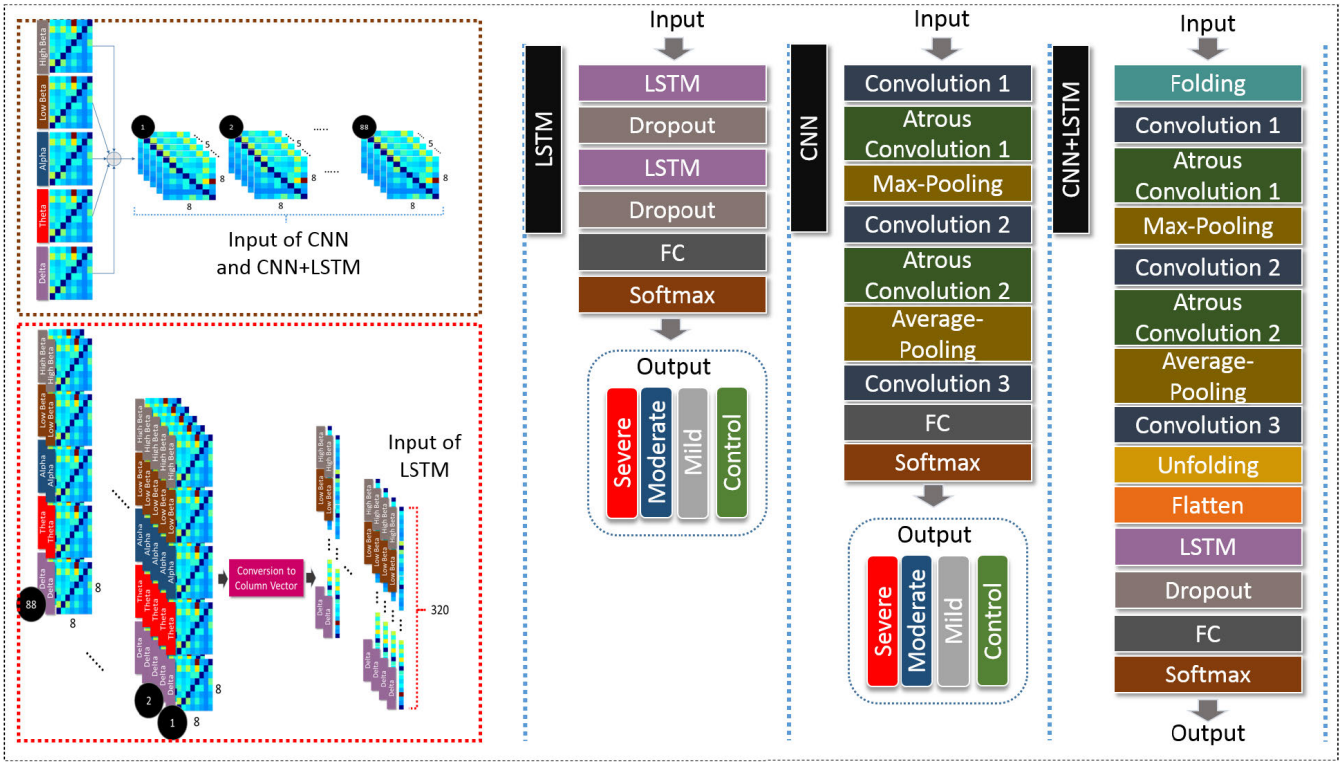

FIGURE 3. Pipeline architecture for training the proposed deep learning structure, CNN, LSTM, and hybrid structure (CNN + LSTM) in the classification of 3-class SAD and HC using 8 by 8 EC matrices from DMN. The two far left diagrams illustrate arrangement of EC matrices as the inputs to CNN, CNN + LSTM and LSTM for 88 subjects, extracted from 5 frequency bands; delta, theta, alpha, low beta, and high beta.

value, in which the 8×8 input has a stride value of 1. Both the CNN and CNN + LSTM models have three convolution layers and two atrous convolution layers. The specifications of the DL networks are provided in Table 3. In the CNN + LSTM model, the LSTM layer is used to extract temporal features from the CNN feature maps. The output of the LSTM layer is then fed to the fully connected layer, and then to the softmax layer, for SAD prediction.

The total data size is $((8 \times 8 \times 5 \times 60 \times 88)$ (regions $\times$ regions $\times$ epochs $\times$ subjects)) for the averaged EC output of DMN data. Ninety percent of the data was used for training, and 10% was secured for testing. In the case of the LSTM model, the input to the model is a 1×64, which is obtained by reshaping the 8×8 matrix to a 1×64. Each participant has 5 different frequencies, so the final matrix will have the size of $1 \times 64 \times 5 \times 88$. Each row is classified as severe, moderate, mild, or HC. The majority rule is applied to the five rows which represent the (delta, theta, alpha, low beta, and high beta) to get the decision for every participant. In contrast, the CNN and CNN + LSTM models were trained on the size of $8 \times 8 \times 5$ and tested on the same size as only 2D convolutions were applied. To ensure the reproducibility of our analysis, 10-fold cross-validation was employed for model robustness purposes. The initialization of weights was generated using a Glorot initializer. The number of epochs considered was 150. In addition, to avoid network overfitting and save training time the early stopping algorithm was applied in the training phase if the error rate is not reduced after 10 epochs. The batch size we considered was 10 and the learning rate of the ADAM optimizer was set to 0.001 for training acceleration. Moreover, cross-entropy weighted loss was used for all deep models in this study.

G. DATA ANALYSIS

The efficient performance of the classifiers may be investigated by the estimation of sensitivity, specificity, and overall classification precision [61]. These measured parameters are estimated as follows:

$$Accuracy = \frac{TP + TN}{TP + FP + TN + FN} \times 100 \quad (6)$$

$$Sensitivity = \frac{TP}{TP + FN} \times 100 \quad (7)$$

$$Specificity = \frac{TN}{TN + FP} \times 100 \quad (8)$$

where TP determines the true-positive features of the class, TN illustrates the true-negative features of the given class, FP indicates the false-positive features of the class, and FN represents the false-negative features of the given class.

H. STATISTICAL ANALYSIS

All statistical observations are expressed in terms of mean $\pm$ standard deviation. The analysis of mean-variances in our sample included two independent variables (Group:

TABLE 3. Architecture of LSTM, CNN and CNN + LSTM for classification of 3-class SAD and HC using DMN connectivity matrices.

ROI	Network Specifications for DMN (8 × 8) Input					
Layer	LSTM		CNN		LSTM+CNN	
	Type	Size	Type	Size	Type	Size
0	Input	1 × 320	Input	8 × 8 × 5	Input	8 × 8 × 5
1	LSTM Layer_1 (110 Hidden Units)	110	Convolution_1 (3 × 3 filter, 8 maps, stride 1)	8 × 8 × 8	Folding Layer	8 × 8 × 5
2	Dropout Layer (20%)	110	Atrous Convolution_1 (3 × 3 filter, 8 maps, stride 1, rate 2)	8 × 8 × 8	Convolution_1 (3 × 3 filter, 8 maps, stride 1)	8 × 8 × 8
3	LSTM Layer_2 (90 Hidden Units)	90	Max-Pooling (2 × 2 window, stride 1)	7 × 7 × 8	Atrous Convolution_1 (3 × 3 filter, 8 maps, stride 1, rate 2)	8 × 8 × 8
4	Dropout Layer (20%)	90	Convolution_2 (3 × 3 filter, 16 maps, stride 1)	7 × 7 × 16	Max-Pooling (2 × 2 window, stride 1)	7 × 7 × 8
5	Fully Connected Layer	4	Atrous Convolution_2 (3 × 3 filter, 16 maps, stride 1, rate 2)	7 × 7 × 16	Convolution_2 (3 × 3 filter, 16 maps, stride 1)	7 × 7 × 16
6	Softmax Layer	4	Average-Pooling (2 × 2 window, stride 1)	6 × 6 × 16	Atrous Convolution_2 (3 × 3 filter, 16 maps, stride 1, rate 2)	7 × 7 × 16
7			Convolution_3 (3 × 3 filter, 32 maps, stride 1)	6 × 6 × 32	Average-Pooling (2 × 2 window, stride 1)	6 × 6 × 16
8			Fully Connected Layer	1 × 1 × 4	Convolution_3 (3 × 3 filter, 32 maps, stride 1)	6 × 6 × 32
9			Softmax Layer	1 × 1 × 4	Unfolding Layer	6 × 6 × 32
10					Flatten Layer	1152
11					LSTM Layer (110 Hidden Units)	110
12					Dropout Layer (20%)	110
13					Fully Connected Layer	4
14					Softmax Layer	4

severe, moderate, mild, and HC) * (DMN Regions; PCC, rLPC, mPFC,...), and one dependent variable (PDC values)). One-way bi-variate variance analysis (ANOVA) uses F-tests (F) to statistically test the equality of means in the SAD groups and HCs. Additionally, the Eta squared (η^2) was reported to quantify the effect size and how independent variables (SAD groups and DMN regions) have impacted the dependent variable (PDC values) in this experimental analysis as shown in Table 4. The higher values of (F) indicate greater variance between the mean of EC values (PDC) between the SAD groups. The one ANOVA test was applied within subject factor, i.e., we made a comparison be-tween the same frequency band (e.g., delta) from all SAD conditions.

Initially, the localized PDC matrices were averaged across all epochs for each subject and then averaged within each group. To assess EC and to minimize variations in effective connectivity over time, EEG data sequences are first segmented into 60 segments of 3 seconds each. Then, the PDC is implemented on each time-synchronized pair of segments. Next, the average values are obtained for each subject from the 60 sets of effective connections. After obtaining the values of the average connections for each subject, they are averaged over the 22 control subjects, 22 severe subjects, 22 moderate subjects, and 22 mild subjects separately. SPSS (version 25.0.0.0, IBM Corp., Armonk, NY) was used for all statistical analyses. Differences were considered statistically significant if the condition $p < 0.05$ is met.

V. RESULT AND DISCUSSION

In this study, EEG recording signals are used to first evaluate the influence of 3-class SAD on the DMN regions and secondly to classify SAD based on its severity levels.

TABLE 4. Comparison of PDC values for different frequency ranges in HC and SAD groups. Significant differences were found in delta, theta, and alpha only (ANOVA test, $p < 0.05$).

Frequency	Group	Mean	SD	F	p-value	η^2
Delta	Severe	0.131	0.019	11.931	0.001	0.32
	Moderate	0.163	0.034			
	Mild	0.231	0.019			
	Control	0.295	0.089			
Theta	Severe	0.143	0.120	3.937	0.03	0.13
	Moderate	0.182	0.154			
	Mild	0.193	0.099			
	Control	0.241	0.101			
Alpha	Severe	0.110	0.014	13.091	0.01	0.12
	Moderate	0.139	0.031			
	Mild	0.190	0.023			
	Control	0.317	0.079			
Low beta	Severe	0.113	0.026	1.571	0.296	0.11
	Moderate	0.111	0.087			
	Mild	0.109	0.021			
	Control	0.114	0.070			
High beta	Severe	0.201	0.036	0.310	0.746	0.07
	Moderate	0.210	0.17			
	Mild	0.219	0.10			
	Control	0.211	0.081			

The method of analysis and classification of SAD utilized EC as the extracted features from EEG signals obtained from 8 ROIs covering the DMN. The results presented in this section comprises analysis on the influence of SAD on DMN regions and performance evaluation on the classification of SAD severity levels and HC using 3 deep learning models.

A. STATISTICAL ANALYSIS OF EFFECTIVE CONNECTIVITY BETWEEN THE SAD AND HC GROUPS

Effective connectivity analysis was performed on the localized artifact-free time series to calculate the mean EEG activation in three DMN brain sources (PCC/Precuneus (BA 7),

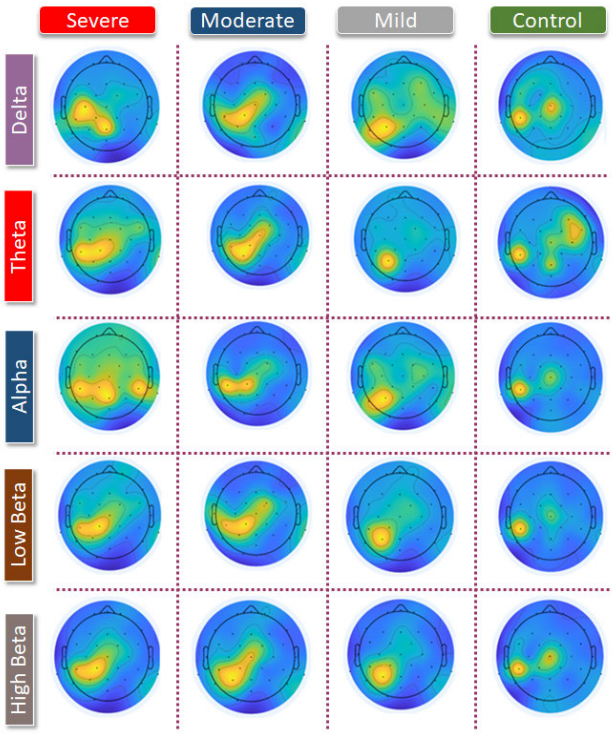

FIGURE 4. Topological maps of the mean total EC for all three SAD groups and HCs in 5 frequency bands. Yellow indicates a greater causal effect, while blue indicates a smaller causal effect.

LPC (BA 39/40), and mPFC (BA 8, 9/10)). In the first experiment, the EC was calculated over the HC, mild, moderate, and severe SAD groups, after which, it was averaged within the subjects of each group. Subsequently, these EC values were estimated into the different frequency rhythms. The results in Table 4 indicate significant differences among the three SAD groups (severe, moderate, mild), and HC) in delta, alpha, and theta bands, $F(3, 252) = 11.931$, $p < 0.001$, $\eta 2 = 0.32$, $F(3, 252) = 13.091$, $p < 0.01$, $\eta^2 = 0.12$, and $F(3, 252) = 3.937$, $p < 0.03$, $\eta^2 = 0.13$, respectively. Contrary to the alpha, delta, and theta bands, no significant differences were observed in the high beta $F(3, 252) = 1.571$, $p < 0.296$, $\eta^2 = 0.11$ and low beta $F(3, 252) = 0.310$, $p < 0.746$, $\eta^2 = 0.07$.

The results in Fig. 4 represent the topographic maps of the averaged peak activity of EC and the activated areas associated with multiclass of SAD (severe, moderate, mild) and HC class in five different frequency bands (delta, theta, alpha, low beta, and high beta). The eight ROIs that belong to the DMN circuit were found to be active and show recognizable EEG activity. The multiple cortical sources of brain EC have been localized by the geometrical registration system (structural MRI scans) provided in the brainstorm toolbox [62]. Fig. 5 proved that precuneus is the most active region in severe and moderate SAD groups compared to HC and mild groups. HC individuals have shown higher information flow in the central mPFC region compared to the other groups, which indicates higher cognitive functions. Mild and

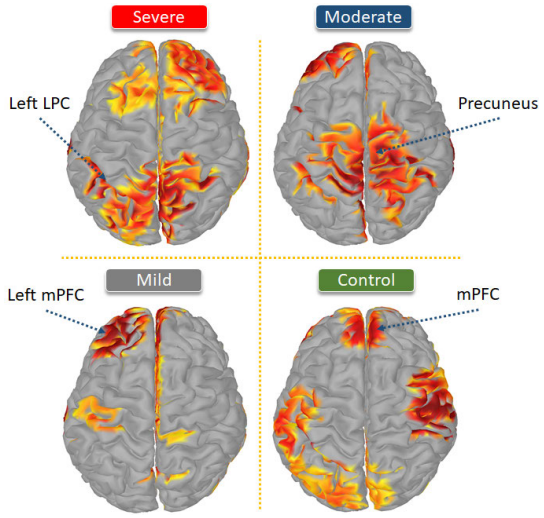

FIGURE 5. Visualization of the computed EC source from EEG activity in the alpha band. It represents the highest 30% of EC values at significant level, $p < 0.05$.

moderate groups have shown greater information flow in the left mPFC than the other groups. The data represented in Fig. 5 are taken from the alpha band due to its ability to detect mental illness and emotion recognition.

B. PERFORMANCE ANALYSIS OF CLASSIFICATION OF 3-CLASS SAD AND HC USING DEEP LEARNING MODELS

In this section, we present the performance of the 3 deep learning architectures, LSTM, CNN, and CNN + LSTM in the classification of SAD and HC using EC extracted from DMN regions. Table 5 presents the classification accuracy for various deep classifiers using EC features in the CNN, LSTM, and CNN + LSTM models, and the combination of these features by the temporal location of EEG regions in the DMN. We found that CNN + LSTM fusion outperformed models based on CNN or LSTM alone in classifying EEG connectivity for SAD groups and HC in all frequency bands.

Among the classification models, the DL based on weighted-average fusion (CNN + LSTM) reveals excellent findings over LSTM, which was trained on EC features alone, achieving an average accuracy of 93% compared to the LSTM accuracy of 86% and CNN accuracy 88%. Therefore, the high classification accuracy obtained by the proposed CNN + LSTM model emphasizes that the extracted EC features from DMN regions can capture unique characteristics that are beneficial for distinguishing between HC and SAD classes. The proposed CNN + LSTM, which includes information flow amongst DMN nodes, is believed to further enhance the classification more than the other models. The SAD and HC classes were predicted using the widespread neuronal activity in the DMN resting-state. Thus, classification accuracy, sensitivity, and specificity obtained were satisfying and agreed with previous neuroimaging studies that used machine learning to predict SAD in the context of resting-state and stimuli-related tasks. Moreover, as far as we

TABLE 5. Performance of the trained DL models (expressed in %) for classification of 3-class SAD vs. HC using connectivity in DMN.

Deep Model	Evaluation Metrics	SAD level				Average
		Severe	Moderate	Mild	Control	
LSTM	Sensitivity	57.14	71.43	71.43	85.71	71
	Specificity	85.71	90.48	90.48	95.24	90
	Precision	57.14	71.43	71.43	85.71	71
	Accuracy	78.57	85.71	85.71	92.86	86
CNN	Sensitivity	71.43	100.00	75.00	85.71	83
	Specificity	90.48	95.45	95.00	95.24	94
	Precision	71.43	85.71	85.71	85.71	82
	Accuracy	85.71	96.43	89.29	92.86	91
CNN+LSTM	Sensitivity	85.71	85.71	87.50	83.33	86
	Specificity	95.24	95.24	100.00	90.91	95
	Precision	85.71	85.71	100.00	71.43	86
	Accuracy	92.86	92.86	96.43	89.29	93

are aware, the present research is the first to use CNN + LSTM to identify the severity of patients with SAD and HC using information flow between DMN regions.

This paper has two essential contributions: (1) an excellent classification accuracy is achieved by the fusion of the CNN + LSTM classifier model: our method achieved a relatively high accuracy of 92.86%, 92.86%, 96.43%, and 89.29% for the classification of severe, moderate, mild SAD groups and HC, respectively, thus providing a promising potential for SAD diagnosis and identification; (2) the cortical site of the precuneus (PZ) has manifested the greatest prominence in patients with SAD due to its correlation with other brain regions, as shown in Fig. 5, which is in line with the works reported in [63], [64]. Additionally, the reported results revealed that the varied EC was essentially associated with DMN network as shown in Fig. 5. The primary neural pattern of the DMN is the self-referential behavior, which is observed in patients impaired with SAD [65]. Experimentally, the disturbance of DMN in patients with SAD has been identified in previous studies [66]. As a result, our study verified that DMN plays a crucial role in SAD. In one study, patients with SAD had exhibited a suppression in the precuneus during cognitive tasks or performing physical activities [32], [35], [67]. Furthermore, reduced perfusion of the precuneus (PZ) was observed in patients with SAD during the resting-state, which suggests that aberrant EC in the precuneus is associated with the pathophysiological mechanization underlying SAD [68]. Moreover, in our study, other regions located in the DMN, including the mPFC and LP cortices, also showed elevated activity in the resting-state, which is in line with previous findings [68]. Similarly, abnormal resting-state connectivity in the DMN has been reported in various neuropsychiatric disorders, including major depression [69], posttraumatic stress disorder (PTSD) [64], [70], and Alzheimer's [24], [71].

Using 60 subjects for training and 28 subjects for testing, the confusion matrices of the classification performance are shown in Fig 6. From the confusion matrix, all SAD subjects and HC cases achieved better accuracy using CNN + LSTM model with 93%, 95%, and 85% accuracy, sensitivity, and specificity, respectively. Fig. 7 represents the classification model's performance (accuracy) and uncertainty of prediction (loss) curves of the proposed classification model (LSTM + CNN).

In the current work, an investigational model uses brain effective connectivity as an input to a CNN + LSTM achieving high classification performance between the SAD groups and HC subjects. The model used the information flow between DMN regions, which is an essential resting-state network, can be considered as a putative biomarker for SAD diagnosis and can elucidate an informative perception about the pathophysiology of SAD. However, information hidden in different layers of convolution can contribute to enhancing the ability of feature discrimination. The hidden layers are crucial parts of determining the final neural network architecture. Some examples to visualize the feature representation learned by the hidden layers of the proposed deep learning methods are reported in the supplementary file. In this study, we used SAD EEG data to analyze the benefits of extracting and merging multi-level convolutional features from different CNN layers, which are abstract representations of inputs at different levels.

The results of this study show that the computation of DMN neural activity notably enhances the classification performance compared with the other related methods available in the literature as shown in Table 7. Though we used a larger dataset in our model, our proposed technique achieved greater sensitivity and specificity performance compared with other reported studies. One more merit of the applied model is the use of 4 different classes relative to the majority of reported literature which used 2 classes only. These results demonstrate that our method presents a significant improvement in the classification of the severity of SAD based on EEG data.

To support our findings, we have examined the effect of our data by using different models from the literature. We have applied an LSTM model [17] and 2 CNN models [10], [11] to detect the severity of SAD. The classification performance is relatively low compared to our proposed models as shown

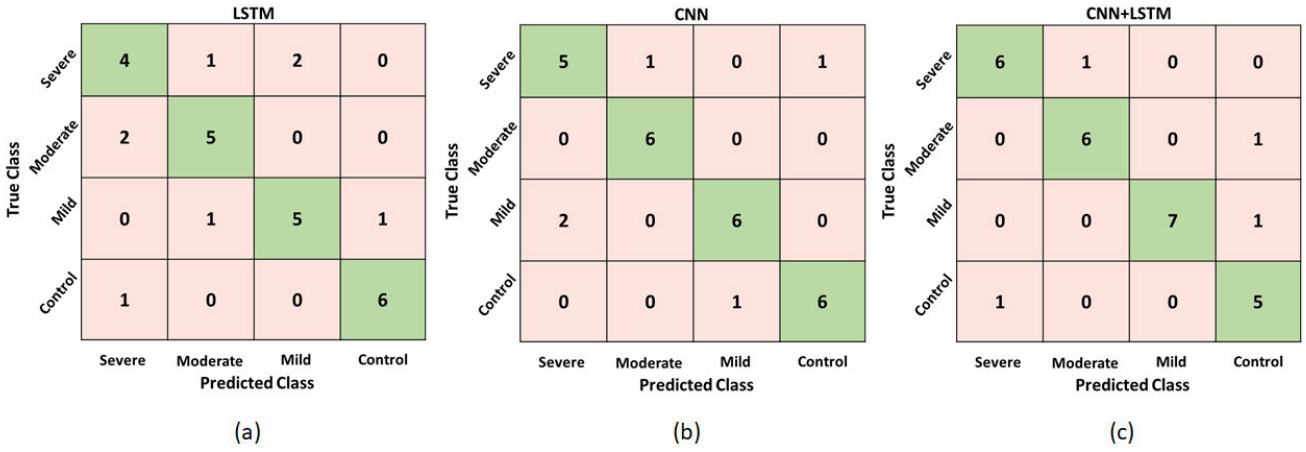

FIGURE 6. Confusion matrix for classification of 3-class SAD test patients and HC test subjects using 3 DL models (a) LSTM, (b) CNN and (c) CNN + LSTM.

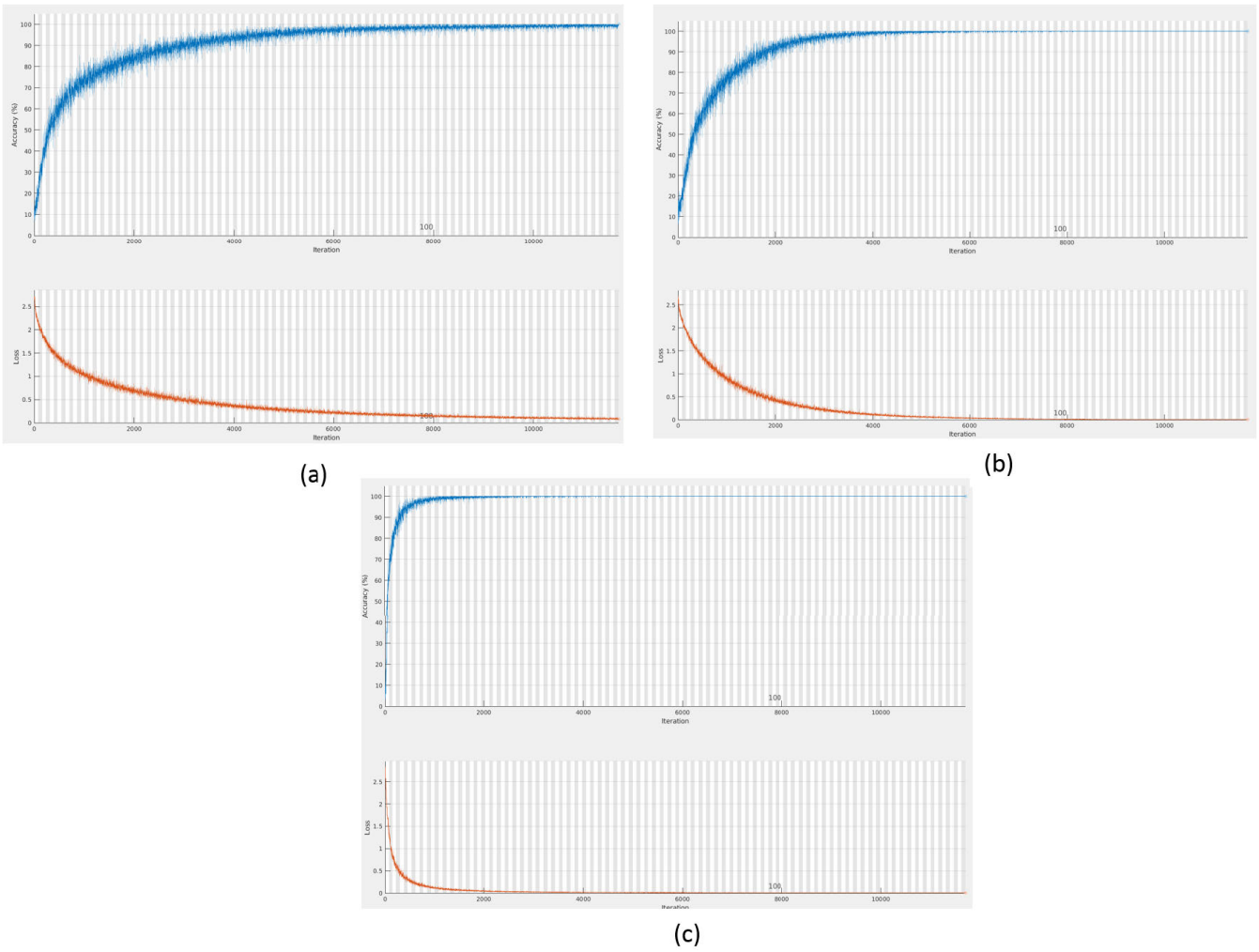

FIGURE 7. Training accuracy and loss curves of 3 DL models (a) CNN, (b) LSTM and (c) CNN + LSTM.

in Table 6. The highest accuracy was achieved by CNN models (81% and 79%). In future research, this method can also be applied to the identification of psychopathology of various brain disorders.

The findings should be considered with regard to their limitations. Specific comorbidities might be detected along with SAD; therefore, these findings may not be restricted to the classification of SAD separately. The implementation

TABLE 6. Comparison between different models in terms of accuracy (expressed in %) for classification of 3-class SAD vs. HC using connectivity in DMN.

Deep Model	Year	Description	SAD level				Average
			Severe	Moderate	Mild	Control	
[17]	2019	LSTM with Attention Mechanism	81.48	81.48	74.07	74.07	77.78
[10]	2019	3-layer CNN	75.86	82.76	82.76	82.76	81.03
[11]	2019	2-layer CNN	75.86	82.76	79.31	79.31	79.31
Our Proposed Method	2021	CNN+LSTM	92.86	92.86	96.43	89.29	93

TABLE 7. Comparison of the proposed technique in terms of accuracy (ACC), sensitivity (SEN) and specificity (SPE) with recent deep learning techniques.

Ref	Year	Feature	Number of Subjects	Number of Classes	Number of Channels	Classifier	ACC (%)	SEN (%)	SPE (%)
[10]	2019	Energy values of signals	64	2	34	CNN	87	79	79
[72]	2020	Raw EEG signals	26	2	16	LSTM	90.82	N/A	N/A
[73]	2020	Frequency & time-domain signals	13	2	16	LSTM	93.27	90	82
Our proposed method	2021	Effective connectivity of DMN	88	4	8	CNN+LSTM	93	95	85

of a cortical connectivity investigation with normal technical instruments may prove to be suboptimal for brain mapping research, thus resulting in poor temporal localization of the EEG activity. Despite these advantages of EEG classification, achieving robust and reliable estimation of the cognitive function of emotional processes using EEG data remains a major challenge. In addition, due to the small applied input features in DMN ($8 \times 8 \times 60$) for each subject, modeling error (overfitting) occurs which has a negative impact on the model performance. To overcome this phenomenon, future studies should use a high density EEG system (64 electrodes or 128 electrodes). There are different spectral features that can be used to classify the severity of SAD, including FFT, wavelet transform, power spectral density, and fuzzy entropy [74]. Future works are encouraged to use fused modality to categorize the severity of SAD (e.g., combining EEG with fNIRS). The fusion between two different neuroimaging techniques is believed to reflect better temporal and spatial characteristics of human brain [75].

VI. CONCLUSION

In this study, it was found experimentally that 88 individuals could be tested for various levels of SAD based on their neural EEG activity. The results in resting-state exhibit a relatively higher degree of causal effects in the DMN regions in SAD groups than in the HC individuals. The hyperactivity of DMN regions in higher severity of SAD indicates neural correlations associated with SAD symptoms severity. Additionally, the results indicated that the activity in those cortical regions that govern sensory and goal-directed processes may represent a crucial factor in SAD diagnosis. In neurophysiology, the EEG-DMN is considered fundamental for identifying the brain dysfunction in SAD in resting-state. This investigation provided evidence that EC-DMN has a good diagnostic potential and can be used as a clinical biomarker for SAD monitoring and treatment. Furthermore, three deep models were utilized to classify the SAD levels, among which, the CNN + LSTM model confirmed the advantage of defining the main DMN regions for SAD classification. Prospectively, the proposed DL model using EC features is believed to create considerable premeditation into the recently developed field of deep learning models for comprehending significative neuroimaging biomarkers.

DISCLOSURE STATEMENT

The authors declare no competing interests.

ACKNOWLEDGMENT

The authors would like to thank the Centre of Graduate Studies of Universiti Teknologi PETRONAS, for providing funding in the form of graduate assistantships.

REFERENCES

[1] A. A. Madison, "Social anxiety symptoms, heart rate variability, and vocal emotion recognition: Evidence of a normative vagally-mediated positivity bias in women," Ph.D. dissertation, Dept. Psychol., Ohio State Univ., Columbus, OH, USA, 2019.
[2] B. Bandelow, D. Baldwin, M. Abelli, C. Altamura, B. Dell'Osso, K. Domschke, N. A. Fineberg, E. Grünblatt, M. Jarema, E. Maron, D. Nutt, S. Pini, M. M. Vaghi, A. Wichniak, G. Zai, and P. Riederer, "Biological markers for anxiety disorders, OCD and PTSD—A consensus statement. Part I: Neuroimaging and genetics," *World J. Biol. Psychiatry*, vol. 17, no. 5, pp. 321–365, Jul. 2016.
[3] D. Beidel, T.-A. Le, and E. Willis, "Social anxiety disorder: An update on diagnostics, epidemiology, etiology, assessment, treatment, unanswered questions, and future directions," in *Pediatric Anxiety Disorders*. Amsterdam, The Netherlands: Elsevier, 2019, pp. 201–223.
[4] B. von Dawans, A. Trueg, C. Kirschbaum, U. Fischbacher, and M. Heinrichs, "Acute social and physical stress interact to influence social behavior: The role of social anxiety," *PLoS ONE*, vol. 13, no. 10, Oct. 2018, Art. no. e0204665.
[5] A. Pittig, J. J. Arch, C. W. R. Lam, and M. G. Craske, "Heart rate and heart rate variability in panic, social anxiety, obsessive–compulsive, and generalized anxiety disorders at baseline and in response to relaxation and hyperventilation," *Int. J. Psychophysiol.*, vol. 87, no. 1, pp. 19–27, Jan. 2013.

[6] A. Al-Ezzi, N. Kamel, I. Faye, and E. Gunaseli, "Review of EEG, ERP, and brain connectivity estimators as predictive biomarkers of social anxiety disorder," *Frontiers Psychol.*, vol. 11, p. 730, May 2020.

[7] H. Crawford, J. Moss, L. Groves, R. Dowlen, L. Nelson, D. Reid, and C. Oliver, "A behavioural assessment of social anxiety and social motivation in fragile X, cornelia de lange and rubinstein-taybi syndromes," *J. Autism Develop. Disorders*, vol. 50, no. 1, pp. 127–144, Jan. 2020.

[8] X.-W. Wang, D. Nie, and B.-L. Lu, "Emotional state classification from EEG data using machine learning approach," *Neurocomputing*, vol. 129, pp. 94–106, Apr. 2014.

[9] L. Bonanni, "The democratic aspect of machine learning: Limitations and opportunities for Parkinson's disease," *Movement Disorders*, vol. 34, no. 2, pp. 164–166, Feb. 2019.

[10] L. S. Mokatren, R. Ansari, A. E. Cetin, A. D. Leow, O. Ajilore, H. Klumpp, and F. T. Y. Vural, "EEG classification based on image configuration in social anxiety disorder," in *Proc. 9th Int. IEEE/EMBS Conf. Neural Eng. (NER)*, Mar. 2019, pp. 577–580.

[11] J. X. Chen, P. W. Zhang, Z. J. Mao, Y. F. Huang, D. M. Jiang, and Y. N. Zhang, "Accurate EEG-based emotion recognition on combined features using deep convolutional neural networks," *IEEE Access*, vol. 7, pp. 44317–44328, 2019.

[12] S. K. Hadjidimitriou and L. J. Hadjileontiadis, "EEG-based classification of music appraisal responses using time-frequency analysis and familiarity ratings," *IEEE Trans. Affect. Comput.*, vol. 4, no. 2, pp. 161–172, Apr. 2013.

[13] K. Samiee, P. Kovacs, and M. Gabbouj, "Epileptic seizure classification of EEG time-series using rational discrete short-time Fourier transform," *IEEE Trans. Biomed. Eng.*, vol. 62, no. 2, pp. 541–552, Feb. 2015.

[14] S. L. Oh, Y. Hagiwara, U. Raghavendra, R. Yuvaraj, N. Arunkumar, M. Murugappan, and U. R. Acharya, "A deep learning approach for Parkinson's disease diagnosis from EEG signals," *Neural Comput. Appl.*, vol. 32, pp. 10927–10933, Aug. 2018.

[15] S. Indolia, A. K. Goswami, S. P. Mishra, and P. Asopa, "Conceptual understanding of convolutional neural network—A deep learning approach," *Procedia Comput. Sci.*, vol. 132, pp. 679–688, Jan. 2018.

[16] Y.-X. Yang, Z.-K. Gao, X.-M. Wang, Y.-L. Li, J.-W. Han, N. Marwan, and J. Kurths, "A recurrence quantification analysis-based channel-frequency convolutional neural network for emotion recognition from EEG," *Chaos, Interdiscipl. J. Nonlinear Sci.*, vol. 28, no. 8, Aug. 2018, Art. no. 085724.

[17] G. Zhang, V. Davoodnia, A. Sepas-Moghaddam, Y. Zhang, and A. Etemad, "Classification of hand movements from EEG using a deep attention-based LSTM network," *IEEE Sensors J.*, vol. 20, no. 6, pp. 3113–3122, Mar. 2020.

[18] A. Salekin, J. W. Eberle, J. J. Glenn, B. A. Teachman, and J. A. Stankovic, "A weakly supervised learning framework for detecting social anxiety and depression," *Proc. ACM Interact., Mobile, Wearable Ubiquitous Technol.*, vol. 2, no. 2, pp. 1–26, Jul. 2018.

[19] N. Nicolaou, S. Hourris, P. Alexandrou, and J. Georgiou, "EEG-based automatic classification of 'awake' versus 'anesthetized' state in general anesthesia using granger causality," *PLoS ONE*, vol. 7, no. 3, Mar. 2012, Art. no. e33869.

[20] A. Frick, M. Gingnell, A. F. Marquand, K. Howner, H. Fischer, M. Kristiansson, S. C. R. Williams, M. Fredrikson, and T. Furmark, "Classifying social anxiety disorder using multivoxel pattern analyses of brain function and structure," *Behavioural Brain Res.*, vol. 259, pp. 330–335, Feb. 2014.

[21] R. L. Buckner and J. L. Vincent, "Unrest at rest: Default activity and spontaneous network correlations," *NeuroImage*, vol. 37, no. 4, pp. 1091–1096, Oct. 2007.

[22] R. L. Buckner, J. R. Andrews-Hanna, and D. L. Schacter, "The brain's default network: Anatomy, function, and relevance to disease," *Ann. New York Acad. Sci.*, vol. 1124, pp. 1–38, Mar. 2008, doi: 10.1196/annals.1440.011.

[23] M. D. Spencer, L. R. Chura, R. J. Holt, J. Suckling, A. J. Calder, E. T. Bullmore, and S. Baron-Cohen, "Failure to deactivate the default mode network indicates a possible endophenotype of autism," *Mol. Autism*, vol. 3, no. 1, pp. 1–9, 2012.

[24] M. D. Greicius, G. Srivastava, A. L. Reiss, and V. Menon, "Default-mode network activity distinguishes Alzheimer's disease from healthy aging: Evidence from functional MRI," *Proc. Nat. Acad. Sci. USA*, vol. 101, no. 13, pp. 4637–4642, Mar. 2004.

[25] Y. I. Sheline, D. M. Barch, J. L. Price, M. M. Rundle, S. N. Vaishnavi, A. Z. Snyder, M. A. Mintun, S. Wang, R. S. Coalson, and M. E. Raichle, "The default mode network and self-referential processes in depression," *Proc. Nat. Acad. Sci. USA*, vol. 106, no. 6, pp. 1942–1947, Feb. 2009.

[26] J. Ding, H. Chen, C. Qiu, W. Liao, J. M. Warwick, X. Duan, W. Zhang, and Q. Gong, "Disrupted functional connectivity in social anxiety disorder: A resting-state fMRI study," *Magn. Reson. Imag.*, vol. 29, no. 5, pp. 701–711, Jun. 2011.

[27] C. Andreescu, L. K. Sheu, D. Tudorascu, S. Walker, and H. Aizenstein, "The ages of anxiety-differences across the lifespan in the default mode network functional connectivity in generalized anxiety disorder," *Int. J. Geriatric Psychiatry*, vol. 29, no. 7, pp. 704–712, Jul. 2014.

[28] A. C. Chen and A. Etkin, "Hippocampal network connectivity and activation differentiates post-traumatic stress disorder from generalized anxiety disorder," *Neuropsychopharmacology*, vol. 38, no. 10, pp. 1889–1898, Sep. 2013.

[29] Y. Tao, B. Liu, X. Zhang, J. Li, W. Qin, C. Yu, and T. Jiang, "The structural connectivity pattern of the default mode network and its association with memory and anxiety," *Frontiers Neuroanatomy*, vol. 9, p. 152, Nov. 2015.

[30] C. F. Beckmann, M. DeLuca, J. T. Devlin, and S. M. Smith, "Investigations into resting-state connectivity using independent component analysis," *Phil. Trans. Roy. Soc. B, Biol. Sci.*, vol. 360, no. 1457, pp. 1001–1013, May 2005.

[31] N. D. Woodward and C. J. Cascio, "Resting-state functional connectivity in psychiatric disorders," *JAMA Psychiatry*, vol. 72, no. 8, pp. 743–744, 2015.

[32] M. D. Fox, A. Z. Snyder, J. L. Vincent, M. Corbetta, D. C. Van Essen, and M. E. Raichle, "The human brain is intrinsically organized into dynamic, anticorrelated functional networks," *Proc. Nat. Acad. Sci. USA*, vol. 102, no. 27, pp. 9673–9678, 2005.

[33] K. N. Ochsner, J. A. Silvers, and J. T. Buhle, "Functional imaging studies of emotion regulation: A synthetic review and evolving model of the cognitive control of emotion," *Ann. New York Acad. Sci.*, vol. 1251, no. 1, pp. E1–E24, Mar. 2012.

[34] W. Liao, H. Chen, Y. Feng, D. Mantini, C. Gentili, Z. Pan, J. Ding, X. Duan, C. Qiu, S. Lui, Q. Gong, and W. Zhang, "Selective aberrant functional connectivity of resting state networks in social anxiety disorder," *NeuroImage*, vol. 52, no. 4, pp. 1549–1558, Oct. 2010.

[35] C. Gentili, E. Ricciardi, M. I. Gobbini, M. F. Santarelli, J. V. Haxby, P. Pietrini, and M. Guazzelli, "Beyond amygdala: Default mode network activity differs between patients with social phobia and healthy controls," *Brain Res. Bull.*, vol. 79, no. 6, pp. 409–413, Aug. 2009.

[36] K. E. Prater, A. Hosanagar, H. Klumpp, M. Angstadt, and K. L. Phan, "Aberrant amygdala–frontal cortex connectivity during perception of fearful faces and at rest in generalized social anxiety disorder," *Depression Anxiety*, vol. 30, no. 3, pp. 234–241, Mar. 2013.

[37] S. Dodhia, A. Hosanagar, D. A. Fitzgerald, I. Labuschagne, A. G. Wood, P. J. Nathan, and K. L. Phan, "Modulation of resting-state amygdala-frontal functional connectivity by oxytocin in generalized social anxiety disorder," *Neuropsychopharmacology*, vol. 39, no. 9, pp. 2061–2069, Aug. 2014.

[38] A. Peterson, J. Thome, P. Frewen, and R. A. Lanius, "Resting-state neuroimaging studies: A new way of identifying differences and similarities among the anxiety disorders?" *Can. J. Psychiatry*, vol. 59, no. 6, pp. 294–300, Jun. 2014.

[39] C. Qiu, W. Liao, J. Ding, Y. Feng, C. Zhu, X. Nie, W. Zhang, H. Chen, and Q. Gong, "Regional homogeneity changes in social anxiety disorder: A resting-state fMRI study," *Psychiatry Res., Neuroimag.*, vol. 194, no. 1, pp. 47–53, Oct. 2011.

[40] S. A. Anteraper, C. Triantafyllou, A. T. Sawyer, S. G. Hofmann, J. D. Gabrieli, and S. Whitfield-Gabrieli, "Hyper-connectivity of subcortical resting-state networks in social anxiety disorder," *Brain Connectivity*, vol. 4, no. 2, pp. 81–90, Mar. 2014.

[41] Y. Kir, D. Sayar-Akaslan, E. Agtas-Ertan, A. Kusman, N. Baskak, Z. Baran, K. Munir, and B. Baskak, "Cortical activity during social acceptance and rejection task in social anxiety disorder: A controlled functional near infrared spectroscopy study," *Prog. Neuro-Psychopharmacology Biol. Psychiatry*, vol. 104, Jan. 2021, Art. no. 110012.

[42] O. David, S. J. Kiebel, L. M. Harrison, J. Mattout, J. M. Kilner, and K. J. Friston, "Dynamic causal modeling of evoked responses in EEG and MEG," *NeuroImage*, vol. 30, no. 4, pp. 1255–1272, May 2006.

[43] M. I. Garrido, J. M. Kilner, S. J. Kiebel, and K. J. Friston, "Evoked brain responses are generated by feedback loops," *Proc. Nat. Acad. Sci. USA*, vol. 104, no. 52, pp. 20961–20966, Dec. 2007.
[44] R. J. Moran, M. Symmonds, K. E. Stephan, K. J. Friston, and R. J. Dolan, "An *in vivo* assay of synaptic function mediating human cognition," *Current Biol.*, vol. 21, no. 15, pp. 1320–1325, Aug. 2011.
[45] C. W. Granger, "Investigating causal relations by econometric models and cross-spectral methods," *Econometrica, J. Econ. Soc.*, vol. 37, pp. 424–438, Aug. 1969.
[46] A. Al-Ezzi, N. Yahya, N. Kamel, I. Faye, K. Alsaih, and E. Gunaseli, "Social anxiety disorder evaluation using effective connectivity measures: EEG phase slope index study," in *Proc. IEEE-EMBS Conf. Biomed. Eng. Sci. (IECBES)*, Mar. 2021, pp. 120–125.
[47] K. J. Friston, L. Harrison, and W. Penny, "Dynamic causal modelling," *NeuroImage*, vol. 19, no. 4, pp. 1273–1302, Aug. 2003.
[48] M. Ding, Y. Chen, and S. L. Bressler, "17 granger causality: Basic theory and application to neuroscience," in *Handbook of Time Series Analysis: Recent Theoretical Developments and Applications*, vol. 437. Hoboken, NJ, USA: Wiley, 2006.
[49] A. K. Seth, A. B. Barrett, and L. Barnett, "Granger causality analysis in neuroscience and neuroimaging," *J. Neurosci.*, vol. 35, no. 8, pp. 3293–3297, Feb. 2015.
[50] A. Al-Ezzi, N. K. Selman, I. Faye, and E. Gunaseli, "Electrocortical brain oscillations and social anxiety disorder: A pilot study of frontal alpha asymmetry and delta-beta correlation," *J. Phys., Conf. Ser.*, vol. 1529, May 2020, Art. no. 052037.
[51] A. Al-Ezzi, N. Kamel, I. Faye, and E. Gunaseli, "Analysis of default mode network in social anxiety disorder: EEG resting-state effective connectivity study," *Sensors*, vol. 21, p. 4098, 2021, doi: 10.3390/s21124098.
[52] W. M. Association, "World medical association declaration of Helsinki: Ethical principles for medical research involving human subjects," *JAMA*, vol. 310, no. 20, pp. 2191–2194, Nov. 2013.
[53] K. Mahjoory, V. V. Nikulin, L. Botrel, K. Linkenkaer-Hansen, M. M. Fato, and S. Haufe, "Consistency of EEG source localization and connectivity estimates," *NeuroImage*, vol. 152, pp. 590–601, May 2017.
[54] F. Tadel, E. Bock, G. Niso, J. C. Mosher, M. Cousineau, D. Pantazis, R. M. Leahy, and S. Baillet, "MEG/EEG group analysis with brainstorm," *Frontiers Neurosci.*, vol. 13, p. 76, Feb. 2019.
[55] C. Imperatori, B. Farina, M. I. Quintiliani, A. Onofri, P. C. Gattinara, M. Lepore, V. Gnoni, E. Mazzucchi, A. Contardi, and G. D. Marca, "Aberrant EEG functional connectivity and EEG power spectra in resting state post-traumatic stress disorder: A sLORETA study," *Biol. Psychol.*, vol. 102, pp. 10–17, Oct. 2014.
[56] M. S. Hämäläinen and R. J. Ilmoniemi, "Interpreting magnetic fields of the brain: Minimum norm estimates," *Med. Biol. Eng. Comput.*, vol. 32, no. 1, pp. 35–42, Jan. 1994.
[57] D. Fraiman and R. Fraiman, "An ANOVA approach for statistical comparisons of brain networks," *Sci. Rep.*, vol. 8, no. 1, pp. 1–14, Dec. 2018.
[58] L. A. Baccalá and K. Sameshima, "Partial directed coherence: A new concept in neural structure determination," *Biol. Cybern.*, vol. 84, no. 6, pp. 463–474, May 2001.
[59] F. Vaz, P. G. de Oliveira, and J. Principe, "A study on the best order for autoregressive EEG modelling," *Int. J. Bio-Medical Comput.*, vol. 20, nos. 1–2, pp. 41–50, Jan. 1987.
[60] A. Al-Ezzi, N. Kamel, I. Faye, and E. G. M. Ebenezer, "EEG frontal theta-beta ratio and frontal midline theta for the assessment of social anxiety disorder," in *Proc. 10th IEEE Int. Conf. Control Syst., Comput. Eng. (ICCSCE)*, Aug. 2020, pp. 107–112.
[61] S. Siuly, E. Kabir, H. Wang, and Y. Zhang, "Exploring sampling in the detection of multicategory EEG signals," *Comput. Math. Methods Med.*, vol. 2015, pp. 1–12, Jan. 2015.
[62] F. Tadel, S. Baillet, J. C. Mosher, D. Pantazis, and R. M. Leahy, "Brainstorm: A user-friendly application for MEG/EEG analysis," *Comput. Intell. Neurosci.*, vol. 2011, pp. 1–13, Oct. 2011.
[63] F. Liu, W. Guo, J.-P. Fouche, Y. Wang, W. Wang, J. Ding, L. Zeng, C. Qiu, Q. Gong, W. Zhang, and H. Chen, "Multivariate classification of social anxiety disorder using whole brain functional connectivity," *Brain Struct. Function*, vol. 220, no. 1, pp. 101–115, Jan. 2015.
[64] T. J. Akiki, C. L. Averill, K. M. Wrocklage, J. C. Scott, L. A. Averill, B. Schweinsburg, A. Alexander-Bloch, B. Martini, S. M. Southwick, J. H. Krystal, and C. G. Abdallah, "Default mode network abnormalities in posttraumatic stress disorder: A novel network-restricted topology approach," *NeuroImage*, vol. 176, pp. 489–498, Aug. 2018.
[65] B. Anderson, P. R. Goldin, K. Kurita, and J. J. Gross, "Self-representation in social anxiety disorder: Linguistic analysis of autobiographical narratives," *Behav. Res. Therapy*, vol. 46, no. 10, pp. 1119–1125, Oct. 2008.
[66] F. Liu, C. Zhu, Y. Wang, W. Guo, M. Li, W. Wang, Z. Long, Y. Meng, Q. Cui, L. Zeng, Q. Gong, W. Zhang, and H. Chen, "Disrupted cortical hubs in functional brain networks in social anxiety disorder," *Clin. Neurophysiol.*, vol. 126, no. 9, pp. 1711–1716, Sep. 2015.
[67] M. D. Greicius, B. Krasnow, A. L. Reiss, and V. Menon, "Functional connectivity in the resting brain: A network analysis of the default mode hypothesis," *Proc. Nat. Acad. Sci. USA*, vol. 100, no. 1, pp. 253–258, Jan. 2003.
[68] D. A. Gusnard and M. E. Raichle, "Searching for a baseline: Functional imaging and the resting human brain," *Nature Rev. Neurosci.*, vol. 2, no. 10, pp. 685–694, Oct. 2001.
[69] Y. Zhang, W. Wu, R. T. Toll, S. Naparstek, A. Maron-Katz, M. Watts, J. Gordon, J. Jeong, L. Astolfi, E. Shpigel, and P. Longwell, "Identification of psychiatric disorder subtypes from functional connectivity patterns in resting-state electroencephalography," *Nature Biomed. Eng.*, vol. 5, no. 4, pp. 309–323, 2020.
[70] R. T. Toll, W. Wu, S. Naparstek, Y. Zhang, M. Narayan, B. Patenaude, C. De Los Angeles, K. Sarhadi, N. Anicetti, P. Longwell, and E. Shpigel, "An electroencephalography connectomic profile of posttraumatic stress disorder," *Amer. J. Psychiatry*, vol. 177, no. 3, pp. 233–243, 2020.
[71] F. Duan, Z. Huang, Z. Sun, Y. Zhang, Q. Zhao, A. Cichocki, Z. Yang, and J. Sole-Casals, "Topological network analysis of early Alzheimer's disease based on resting-state EEG," *IEEE Trans. Neural Syst. Rehabil. Eng.*, vol. 28, no. 10, pp. 2164–2172, Oct. 2020.
[72] B. Penchina, A. Sundaresan, S. Cheong, and A. Martel, "Deep LSTM recurrent neural network for anxiety classification from EEG in adolescents with autism," in *Proc. Int. Conf. Brain Informat.* Cham, Switzerland: Springer, 2020, pp. 227–238.
[73] B. Penchina, A. Sundaresan, S. Cheong, V. Grace, A. Valero-Cabré, and A. Martel, "Evaluating deep learning EEG-based anxiety classification in adolescents with autism for breathing entrainment BCI," Tech. Rep., 2020.
[74] J. Sun, R. Cao, M. Zhou, W. Hussain, B. Wang, J. Xue, and J. Xiang, "A hybrid deep neural network for classification of schizophrenia using EEG data," *Sci. Rep.*, vol. 11, no. 1, pp. 1–16, Dec. 2021.
[75] F. Al-Shargie, M. Kiguchi, N. Badruddin, S. C. Dass, A. F. M. Hani, and T. B. Tang, "Mental stress assessment using simultaneous measurement of EEG and fNIRS," *Biomed. Opt. Exp.*, vol. 7, no. 10, pp. 3882–3898, 2016.

ABDULHAKIM AL-EZZI received the bachelor's and master's degrees in biomedical engineering from Universiti Tun Hussein Onn Malaysia (UTHM). He is currently pursuing the Ph.D. degree with Universiti Teknologi PETRONAS. His research interests include the development of emotion, emotion regulation, temperament in patients with anxiety and depression by using psychophysiological, neurobiological, and behavioral measures, delineating cognitive endophenotypes of anxiety disorders, and computational neuroscience with an affirmation on machine learning, deep learning, and statistical analysis.

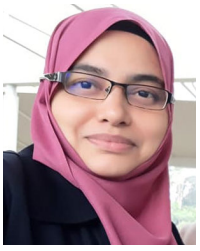

NORASHIKIN YAHYA (Member, IEEE) received the B.Eng. degree (Hons.) in electronic engineering from The University of Sheffield, U.K., in 2001, the M.Sc. degree in electrical engineering from Lehigh University, USA, in 2004, and the Ph.D. degree in electrical engineering from Universiti Teknologi PETRONAS (UTP), Malaysia, in 2015. She currently holds a position of Senior Lecturer with UTP and also a member of the Centre for Intelligent Signal and Imaging Research (CISIR) Laboratory, one of the National Higher Institution Centre of Excellence (HICoE) status focusing on neuro signal and image analysis as its research niche area. Her current research interests include image segmentation and pattern recognition, involving biomedical signals and images using deep learning architecture.

NIDAL KAMEL (Senior Member, IEEE) received the Ph.D. degree (Hons.) from the Technical University of Gdansk, Poland, in 1993. His Ph.D. work was focused on subspace-based array signal processing for direction-of-arrival estimation. Since 1993, he has been involved in research projects related to estimation theory, noise reduction, optimal filtering, and pattern recognition. He is currently an Associate Professor with Universiti Teknologi PETRONAS. His current research interests include brain signal and image processing using electroencephalography (EEG), fMRI, MRI, and fNIR for diagnosis and quantitative assessment of various brain disorders, including stress, anxiety, and MDD, image processing for background initialization and visual periodic motion estimation and magnification.

IBRAHIMA FAYE (Senior Member, IEEE) received the B.Sc., M.Sc. and Ph.D. degrees in mathematics from the University of Toulouse and the M.Sc. degree in engineering of medical and biotechnological data from École Centrale Paris. He is currently an Associate Professor at Universiti Teknologi PETRONAS, Seri Iskandar, Malaysia. He is attached to the Department of Fundamental and Applied Sciences and the Centre for Intelligent Signal and Imaging Research (CISIR), a national centre of excellence. His research interests include machine learning, mathematics, signal and image processing, and science of learning. He has published over 150 articles in peer-reviewed journals and international conferences and holds two patents in image processing. He is currently the Vice-Chair of the IEEE Computational Intelligence Society (CIS), Malaysia.

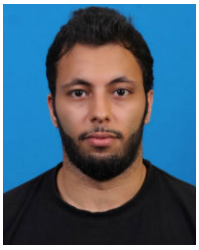

KHALED ALSAIH (Member, IEEE) received the bachelor's degree in electronics engineering majoring in biomedical-instrumentation engineering from Multimedia University, Malaysia, in 2014, the joint master's double degree in computer vision, robotics, and mechatronics from the University of Technology Malaysia and Universite Bourgogne Franche-Comté, France, in 2016, and the Ph.D. degree in electrical and electronics engineering from Universiti Teknologi PETRONAS (UTP), Malaysia, in 2020. He currently holds a postdoctoral position at the Laboratoire Hubert Curien, Université de Lyon, Saint-Etienne, France. His research interests include artificial intelligence, retinal disease segmentation and classification, image and signal processing, medical imaging, and deep learning.

ESTHER GUNASELI received the bachelor's degree in medicine and surgery (M.B.B.S.) from the Stanley Medical College, India, in 1990, the Psychological Medicine (M.P.M.) degree from the University of Malaya, Malaysia, in 1996, and the Psychiatry of Age Care Fellowship from The University of Western Australia, Australia, in 2002. She is currently the Head of the Section of Psychiatry Discipline Sub Unit, Universiti Kuala Lumpur Kampus Cawangan Royal College of Medicine Perak. She is a Psychiatrist and has different places of practice at the UniKL Royal College of Medicine, Ipoh; the Hospital Raja Permaisuri Bainun, Ipoh; the KPJ Ipoh Specialist Hospital, Ipoh; and the Pantai Hospital Ipoh. She is actively teaching and supervising postgraduate student's research work. Her research interest includes brain sciences to understand psychological conditions better, especially in elders.